A Data-Driven Koopman Approach for Power System Nonlinear Dynamic Observability Analysis

Yijun Xu, *Senior Member*, Qinling Wang, *Student Member*, Lamine Mili, *Life Fellow*, Zongsheng Zheng, *Member*, Wei Gu, *Senior Member*, Shuai Lu, *Member*, Zhi Wu, *Senior Member*

***Abstract*—A prerequisite to dynamic state estimation of a stochastic nonlinear dynamic model of a power system is its observability analysis. However, due to the model nonlinearity, the traditional methods either suffer from a poor estimation accuracy if a linear approximation is performed or yield an extremely complicated procedure if the Lie-derivative method is applied to a large-scale power system. To address these weaknesses, we propose a new data-driven Koopman-based observability method by revealing the link that exists between the Koopman operator and the Lie-derivative in the Koopman canonical coordinates. This enables the proposed data-driven method not only to be fully *derivative-free*, which alleviates its implementation complexity but also overcomes the model nonlinearity and inaccuracy of the system. Furthermore, as an important byproduct, the proposed observability analysis scheme provides a valuable guide for the selection of the *observables* of the Koopman operator, which is a major difficulty for the application of this operator. Finally, we demonstrate the excellent performance of the proposed method on several IEEE standard test systems.**

***Index Terms*—Observability analysis; Power system dynamics; Data-driven Koopman operator; Degree of observability; Dynamic state estimation.**

I. Introduction

OBSERVABILITY analysis of a system is a prerequisite to its state estimation since it characterizes the capability of inferring its internal states through the measurement data [1]. Observability analysis methods of a power system with SCADA measurements have been well documented in the literature. More recently, observability analysis has been extended to phasor measurement units (PMUs) [2]–[10]. The first paper addressing this problem was authored by Baldwin, Mili *et al.* [2], which proposed a graph-theoretic approach to find the minimum PMU placement. Nuqui and Phadke [3] further extended this work by introducing the concept of depth of unobservability. Gou *et al.* [4] unified the observability analysis in static state estimation and bad data detection. Gou *et al.* [5] proposed a sparse factorization-based strategy to improve system observability. Later, Liao [6] initiated the fault location observability with an impedance-based technique while Korkali and Abur [7] suggested a traveling-wave-based method to satisfy the observability of a power system at the fault location. Due to the growing installation of measurement devices on the power distribution systems, some of the developed observability methods for transmission systems have been extended to these systems [8], [9], [11], [12].

Following the increasing deployment of PMUs in power systems, the observability analysis of power system nonlinear dynamic models has recently attracted the attention of power researchers. These models are characterized by nonlinear differential-algebraic equations involving time-dependent nonlinear functions [13]. Observability analysis methods based on linear approximation were first proposed in the literature. Obviously, their accuracy becomes poor when the system nonlinearities become strong [14]. Wang *et al.* [15] were the first to address this problem by proposing a Lie-derivative-based method of a nonlinear power system model using the classical generator model. Later, Rouhani and Abur [14] further extend this approach to a decentralized power system model using a synchronous generator model with the IEEE-Type 1 exciter. Unfortunately, while the Lie-derivative method yields good results for nonlinear dynamic models, it becomes extremely complicated for medium or large-size systems. To overcome this difficulty, non-derivative-based approaches have been initiated. One popular method is the empirical observability Gramian method advocated by Qi *et al.* [13]. Interestingly, in addition to its easy implementation, it is capable to assess the degree of system observability. Recently, Zheng $et\ al.$ [16] proposed a polynomial-chaos-based method able to assess the degree of observability, e.g., the *puny* and *brawny* observability, for a stochastic nonlinear dynamic model. Then, they extended this method to both decentralized and centralized power system dynamic models in [16], [17]. Here, it is worth mentioning that assessing the degree of observability of a power system dynamic model allows us to determine the accuracy of a dynamic state estimator (DSE) as reported by the associated IEEE Task Force recently in [18]. Typically, a larger degree of observability leads to a more accurate DSE, and vice versa. Also, it can assist in the proper selection of the measurements as addressed by Rouhani and Abur [14] as well as their optimal placement as investigated by Qi *et al.* [13].

Particularly, we would like to point out that all the above-mentioned observability analysis methods are model-based methods while the power system model discrepancies and parameter uncertainties do exist and, sometimes, can not be ignored [19]–[23]. Therefore, an alternative strategy to deal

Y. Xu, Q. Wang, W. Gu, S. Lu, and Z. Wu are with the Electrical Engineering Department, Southeast University, Nanjing, Jiangsu 210096, China, (e-mail:{yijunxu, qlingwang, wgu, zwu}@seu.edu.cn).

L. Mili is with the Bradley Department of Electrical and Computer Engineering, Virginia Tech, Northern Virginia Center, Falls Church, VA 22043 USA (e-mail:{lmili}@vt.edu).

Z. Zheng is with the College of Electrical Engineering, Sichuan University, Chengdu, 610065 China (e-mail: zongsheng56@126.com).

The study was supported by the science and technology project of the State Grid Corporation of China, Grant 5108-202218280A-2-366-XG. *(Corresponding author: Wei Gu.)*

with this issue is to rely on a data-driven approach, which does not appear in the existing literature yet. This has motivated us to develop a data-driven Koopman-operator-based approach, whose good performance is demonstrated on several IEEE test systems with different generator models.

In summary, the contributions of the paper are as follows:

- Since the measurement selection plays a key role in the observability of a power system, we propose to combine this selection with the nonlinear dynamical state model to get an extended model to which the Koopman operator is applied in a data-driven manner.
- To avoid the complicated derivative procedure of the derivative-based observability analysis ([14], [15]) and to alleviate the computational burden of this analysis, we develop an observability method that is fully *derivative-free* while preserving the nonlinearity of the model.
- To overcome the problem of selecting *the observables* for the Koopman operator, we propose to choose them based on the derived Koopman observability matrix since its associated degree of observability can provide valuable guidance for that task.
- Very importantly, it is shown that measurements contribute differently to the degree of observability of a dynamical system, some more than others.
- Finally, in addition to applying our proposed approach to the traditional synchronous generator-based power system, we apply it to the a system with converter-interfaced generation with virtual inertia control. To our knowledge, it is the first time this application has been reported in a paper.

This paper is organized as follows. Section II formulates the problem of the power system dynamic observability analysis. Section III provides the background on the Koopman operator. Section IV presents the proposed Koopman-based observability analysis. Section V presents case studies. Finally, Section VI concludes the paper and highlights some future work.

II. Preliminaries of Observability Analysis

In this section, we will first briefly introduce the traditional observability analysis for a linear time-invariant system. Then, we generalize it to a nonlinear dynamic power system model.

A. Observability Analysis of a Time-Invariant Linear Dynamical System

Consider a linear time-invariant dynamical system governed by

$$\dot{\boldsymbol{x}}(t) = \boldsymbol{A}\boldsymbol{x}(t) + \boldsymbol{B}\boldsymbol{u}(t), \tag{1a}$$

$$\boldsymbol{y}(t) = \boldsymbol{C}\boldsymbol{x}(t) + \boldsymbol{D}\boldsymbol{u}(t), \tag{1b}$$

where $\boldsymbol{x}(t) \in \mathbb{R}^{n_x \times 1}$, $\boldsymbol{y}(t) \in \mathbb{R}^{n_y \times 1}$ and $\boldsymbol{u}(t) \in \mathbb{R}^{n_u \times 1}$ are the state, the measurement, and the input vectors at time t, respectively; and $\boldsymbol{A}$, $\boldsymbol{B}$, $\boldsymbol{C}$, and $\boldsymbol{D}$ are the constant matrices. This system has an observability matrix, $\boldsymbol{O} \in \mathbb{R}^{(n_x n_y) \times n_x}$, given by

$$\boldsymbol{O} = \begin{bmatrix} \boldsymbol{C} \\ \boldsymbol{C}\boldsymbol{A} \\ \vdots \\ \boldsymbol{C}\boldsymbol{A}^{n_x - 1} \end{bmatrix}. \tag{2}$$

The system is observable if and only if its observability matrix is non-singular [24].

B. Observability Analysis of a Nonlinear Dynamical System

Consider a nonlinear dynamical system governed by

$$\dot{\boldsymbol{x}}(t) = \boldsymbol{f}(\boldsymbol{x}(t)), \tag{3}$$

$$\boldsymbol{y}(t) = \boldsymbol{h}(\boldsymbol{x}(t)), \tag{4}$$

where $\boldsymbol{f} = [f_1(x), \cdots, f_{n_x}(x)]^T$ and $\boldsymbol{h} = [h_1(x), \cdots, h_{n_y}(x)]^T$ are the vector-valued system and observation functions, respectively. More specifically, since we are focusing on a power system dynamical model, $\boldsymbol{f}$ stands for the generator model while $\boldsymbol{h}$ represents the observation model based on the PMU data contained in $\boldsymbol{y}$. These PMUs include measurements of the terminal active and reactive power injections and voltage magnitude and angle, namely P, Q, V, and θ [25], [26]. Also, in this paper, both a classical generator model and a 9th-order synchronous generator with the IEEE-DC1A exciter and the TGOV1 turbine-governor are considered. More details of these system models, $\boldsymbol{f}$, can be found in Sauer, Pai, and Chow [27].

The observability of a system refers to the unique determination of its states from the measurements. The analysis of the observability of a nonlinear dynamic system given by (3) and (4) has been well-documented by control theory researchers [28], [29], and has been recently extended to power systems [14], [15], [17], [18]. Following their work, let us first define its cumulative observation vector, $\mathcal{Y}(t)$, as

$$\mathcal{Y}(t) = \left[\boldsymbol{y}(t), \dot{\boldsymbol{y}}(t), \cdots, \boldsymbol{y}^{(n_x - 1)}(t)\right]^T. \tag{5}$$

Then, let us derive its associated Jacobian matrix, a.k.a. the observability matrix, which is expressed as

$$\boldsymbol{O}(t) = \frac{\partial \mathcal{Y}(t)}{\partial \boldsymbol{x}(t)}. \tag{6}$$

According to the implicit function theorem, this system is locally observable if and only if the Jacobian matrix, $\boldsymbol{O}(t)$, is non-singular, i.e., $\mathrm{rank}(\boldsymbol{O}(t)) = n_x$. This also means that, in the time interval, $[t_0, t_1]$, its initial state, $\boldsymbol{x}(t_0)$, can be uniquely inferred from its measurements, $\mathcal{Y}(t)$, where $t \in [t_0, t_1]$. Note that this Jacobian matrix has been widely used to assess the degree of the observability for a nonlinear dynamic power systems via its associated condition number [14], [15], [17].

Obviously, the calculation of $\boldsymbol{O}(t)$ is not trivial. For simplicity, we may use an observability method based on an approximate linear model, but this will inevitably lead to inaccurate results if the power system is strongly nonlinear, for example, if some of its sections are heavily loaded [14], [15]. To achieve more reliable results, it will be better to rely

on the Lie derivatives as recommended in [14], [15], [29]. Recall that the Lie derivative of $\boldsymbol{h}$ with respect to $\boldsymbol{f}$ is defined as

$$\boldsymbol{L_f h} = \nabla \boldsymbol{h} \cdot \boldsymbol{f}. \tag{7}$$

Its associated jth-order Lie derivatives can be derived using a recursive procedure as follows:

$$\boldsymbol{L_f^j h} = \frac{\partial \boldsymbol{L_f^{j-1} h}}{\partial \boldsymbol{x}} \cdot \boldsymbol{f}, \tag{8}$$

while its cumulative measurement vector is given by

$$\mathcal{Y}(t) = \left[\boldsymbol{L_f^0 h}, \boldsymbol{L_f^1 h}, \cdots, \boldsymbol{L_f^{n_x-1} h}\right]^T, \tag{9}$$

where the zero-order Lie derivative is defined as $\boldsymbol{L_f^0 h} = \boldsymbol{h}$. This yields the observability matrix given by

$$\boldsymbol{O}(t) = \begin{bmatrix} \frac{\partial \boldsymbol{L_f^0 h}}{\partial \boldsymbol{x}} \\ \frac{\partial \boldsymbol{L_f^1 h}}{\partial \boldsymbol{x}} \\ \vdots \\ \frac{\partial \boldsymbol{L_f^{n_x-1} h}}{\partial \boldsymbol{x}} \end{bmatrix}, \tag{10}$$

where

$$\frac{\partial \boldsymbol{L_f^0 h}}{\partial \boldsymbol{x}} = \frac{\partial \boldsymbol{h}}{\partial \boldsymbol{x}}, \frac{\partial \boldsymbol{L_f^j h}}{\partial \boldsymbol{x}} = \frac{\partial \left(\frac{\partial \boldsymbol{L_f^{j-1} h}}{\partial \boldsymbol{x}} \cdot \boldsymbol{f} \right)}{\partial \boldsymbol{x}}. \tag{11}$$

Till now, we can assess the observability of a nonlinear power system dynamic model by checking the rank of the matrix, $\boldsymbol{O}(t)$. Furthermore, that matrix can also provide information on the degree of observability via its condition number. Different applications can select different criteria. For instance, in a typical meter placement design for the state estimation, we can either aim to place the minimum amount of meters to satisfy the basic observability requirement, namely the observability matrix, $\boldsymbol{O}(t)$, has full rank [7], [30], or target to maximize the degree of the system observability given a fixed number of metering devices [13].

Remark 1. *Although the Lie derivative method yields higher accuracy, the time-consuming calculation of the derivatives prohibits its applications to practical power systems [14]. In addition, this model-based method may yield unreliable results if the power system has dynamic industrial loads or intermittent renewable energy resources that are not accounted for in the model, which is typically the case. This problem has prompted us to develop a Lie derivative-free approach that lifts the nonlinear system model into a higher-dimensional linear model, which allows us to use an observability method for linear systems. Such lifting is performed via the Koopman operator as described next.*

III. The Koopman Operator

Uncovered as a spectral operator for nonlinear dynamical systems by Mezić [31] (see also [32] for further details), the Koopman operator was first applied to power systems by Suzuki and Mezić [33], [34] to perform a data-driven coherency identification and stability analysis. Later on, it has further attracted the attention of power researchers for its capability to perform frequency control [35], [36], participation factor approximations [37], and uncertainty quantification [38], to cite a few. In this section, we will first summarize the fundamentals of the Koopman operator and then, we will outline the most common data-driven Koopman numerical methods proposed in the literature.

A. Fundamentals of the Koopman Operator

Let us assume that the autonomous nonlinear system governed by (3) evolves on a finite-dimensional manifold, M, governed by $\boldsymbol{f} : M \to M$. Let us define a scalar-valued, continuous function, $g : M \to \mathbb{R}$, as the so-called *observable function*. Now, given a linear, infinite-dimensional *Koopman operator*, $\mathcal{K}_t$, that acts on g, we have

$$\mathcal{K}_t\, g = g \circ \boldsymbol{S}_t, \tag{12}$$

where $\boldsymbol{S}_t$ is called its flow and is given by

$$\boldsymbol{S}_t : M \to M;\, \boldsymbol{x}(0) \to \boldsymbol{x}(t) = \boldsymbol{x}(0) + \int_0^t \boldsymbol{f}(\boldsymbol{x}(\tau))d\tau. \tag{13}$$

The Koopman eigenvalues, λ_i, and the Koopman eigenfunctions, ϕ_i, are expressed as

$$\mathcal{K}_t \phi_i = e^{\lambda_i t}\phi_i, i = 1, ..., \infty \tag{14}$$

Here, it is worth pointing out that, in practice, by selecting a finite set of observables, $\boldsymbol{g} : M \to \mathbb{R}^{n_d}$, $n_d \geq n_x$, we can estimate a subset of the Koopman eigenvalues, $\{\lambda_i\}_{i=1}^{n_d}$, and eigenfunctions, $\{\phi_i\}_{i=1}^{n_d}$. In this way, n_d elements of $\boldsymbol{g}$ lie within the span of the Koopman eigenfunctions ϕ_i, yielding

$$\boldsymbol{g}(\boldsymbol{x}(t)) = \sum_{i=1}^{n_d} \phi_i(\boldsymbol{x}(t))\, \boldsymbol{v}_i = \sum_{i=1}^{n_d} \phi_i(\boldsymbol{x}(0))\, \boldsymbol{v}_i\, e^{\lambda_i t}, \tag{15}$$

where $\boldsymbol{v}_i \in \mathbb{C}$, $i = 1, ..., n_d$, denote the Koopman modes and $\{\lambda_i, \phi_i, \boldsymbol{v}_i\}_{i=1}^{n_d}$ are known as the Koopman tuples. The Koopman operator allows us to describe the evolution of the system (3) in the linear Koopman canonical coordinates by capturing its dominant nonlinear dynamics. In what follows, we will describe how to approximate the Koopman operator and its associated Koopman tuples.

B. Data-Driven Koopman Operator Approximation

Although there are several existing methods to estimate the Koopman eigenvalues and eigenfunctions, e.g., the dynamic mode decomposition (DMD) method [39], the modified Arnoldi method [32], [33], the extended dynamic mode decomposition (EDMD) method [40], [41], to name a few, we select the EDMD method because it allows us to flexibly define the observables for constructing an augmented Koopman operator as shown in Section IV.

Now, let us briefly describe the main steps of the data-driven EDMD method proposed in [41], which processes n_s sets of snapshot pairs obtained from the recorded data, $\{(\boldsymbol{x}_{k-1}, \boldsymbol{x}_k)\}_{k=1}^{n_s}$. First, we construct two data matrices, $\boldsymbol{X}_0 = [\boldsymbol{X}_0 \cdots \boldsymbol{X}_{n_s-1}]$ and $\boldsymbol{X}_1 = [\boldsymbol{X}_1 \cdots \boldsymbol{X}_{n_s}]$, where $\boldsymbol{X}_0, \boldsymbol{X}_1 \in \mathbb{R}^{n_x \times n_s}$. Then, we build the vector-valued observable functions, $\boldsymbol{g}(\boldsymbol{x}_k) = [g_1(\boldsymbol{x}_k) \cdots g_{n_d}(\boldsymbol{x}_k)]^T$, and the observable matrices, $\boldsymbol{G}_0 = [\boldsymbol{g}_0 \cdots \boldsymbol{g}_{n_s-1}]$ and $\boldsymbol{G}_1 = [\boldsymbol{g}_1 \cdots \boldsymbol{g}_{n_s}]$, where

$\boldsymbol{G}_0, \boldsymbol{G}_1 \in \mathbb{R}^{n_d \times n_s}$ and $n_d \geq n_x$. Then, we construct a matrix, $\boldsymbol{K} \in \mathbb{R}^{n_d \times n_d}$, as

$$\boldsymbol{K} = \boldsymbol{G}_1 \boldsymbol{G}_0^{\dagger}, \tag{16}$$

where $[\cdot]^{\dagger}$ is the Moore-Penrose pseudoinverse. Finally, we calculate the eigenvalues of $\boldsymbol{K}$, denoted as μ_i, which are estimates of the discrete-time Koopman eigenvalues[1]. We also calculate the left-eigenvectors of $\boldsymbol{K}$ and put them in a matrix, $\boldsymbol{L}$. We estimate the Koopman eigenfunctions as

$$\boldsymbol{\phi}(\boldsymbol{x}_k) \approx \boldsymbol{L}\boldsymbol{g}(\boldsymbol{x}_k), \tag{17}$$

where $\boldsymbol{\phi}(\boldsymbol{x}_k) = [\phi_1(\boldsymbol{x}_k) \cdots \phi_{n_d}(\boldsymbol{x}_k)]^T$. To estimate a finite set of Koopman mode approximates, we define a projection matrix, $\boldsymbol{P} \in \mathbb{R}^{n_x \times n_d}$, such that $\boldsymbol{x}_k = \boldsymbol{P}\boldsymbol{g}(\boldsymbol{x}_k)$. Using (17), we get

$$\boldsymbol{x}_k = \boldsymbol{P}\boldsymbol{L}^{-1}\boldsymbol{\phi}(\boldsymbol{x}_k). \tag{18}$$

Then, we estimate the Koopman mode approximates as the column vectors of

$$\boldsymbol{U} = \boldsymbol{P}\boldsymbol{L}^{-1} = \boldsymbol{x}_k \boldsymbol{\phi}(\boldsymbol{x}_k)^{-1}, \tag{19}$$

where $\boldsymbol{U} \in \mathbb{C}^{n_x \times n_d}$. In summary, we have expressed the evolution of the system states as a finite-dimensional linear Koopman expansion given by

$$\boldsymbol{x}_k = \boldsymbol{g}(\boldsymbol{x}_k) \approx \sum_{i=1}^{n_d} \phi_i(\boldsymbol{x}_k)\boldsymbol{v}_i = \sum_{i=1}^{n_q} \phi_i(\boldsymbol{x}_0)\boldsymbol{v}_i \mu_i^k. \tag{20}$$

Here, it is worth mentioning that we can include in the observable vector, $\boldsymbol{g}(\boldsymbol{x})$, any continuous functions of the state variables contained in $\boldsymbol{x}$, including the state variables themselves. Note that the selection of a finite set of observables that result in good estimates of the Koopman modes remains an open problem for most real systems, including power systems. We would like to emphasize that the Koopman method is a typical data-driven method. Indeed, the estimation of the Koopman operator relies exclusively on data, either numerically or via simulations. If the data is obtained through the measurements, such as PMU data, the Koopman method can be referred to as a measurement-based method. Alternatively, if no metered data is directly provided, data obtained from simulations can still be utilized.

Remark 2. *As shown in the literature [33]–[36], [38], the Koopman operator lifts a nonlinear model into a higher-dimension linear one that can be directly analyzed using linear methods. However, this does not naturally apply to our dynamic observability analysis problem since the Koopman operator only applies to the system model given by (3), while another key element for the observability analysis, namely its associated measurement model given by (4), is not included. This will be an important issue that will be addressed next.*

IV. The Proposed Koopman Method for Dynamic Observability Analysis

In this section, we will present our proposed augmented Koopman operator-based dynamic observability analysis. Its associated degree of observability will also be discussed.

[1]Here, μ_i can be computed from the continuous-time Koopman eigenvalues, λ_i, as $\mu_i = e^{\lambda_i \Delta t}$, where Δt denotes the time interval.

A. Augmented Koopman Operator

First, let us denote the observable functions for the original dynamic system model as $\boldsymbol{g}_x(\boldsymbol{x}) \in \mathbb{R}^{n_d}$, yielding

$$\dot{\boldsymbol{g}}_x(\boldsymbol{x}(t)) = \boldsymbol{K}_x \cdot \boldsymbol{g}_x(\boldsymbol{x}(t)), \tag{21}$$

where $\boldsymbol{K}_x \in \mathbb{R}^{n_d \times n_d}$ is the associated Koopman operator. Then, let us formulate an augmented Koopman operator that unifies the system model given by (3) and its measurement model given by (4) into the Koopman canonical coordinates. To do so, we propose to further introduce an extra set of observable functions, $\boldsymbol{g}_y(\boldsymbol{x}) \in \mathbb{R}^{n_y}$, which represent all the measurement functions as given by (4), that is,

$$\boldsymbol{g}_y(\boldsymbol{x}(t)) = \boldsymbol{y}(t) = \boldsymbol{h}(\boldsymbol{x}(t)). \tag{22}$$

The way we select $\boldsymbol{g}_y(\boldsymbol{x})$ simply transforms the measurement functions, $\boldsymbol{h}(\boldsymbol{x})$, into the Koopman space while obtaining a larger set of observables contained in $\boldsymbol{g}(\boldsymbol{x}) = [\boldsymbol{g}_x(\boldsymbol{x})\ \boldsymbol{g}_y(\boldsymbol{x})]^T$, where $\boldsymbol{g}(\boldsymbol{x}) \in \mathbb{R}^{(n_d+n_y)}$. Accordingly, we have

$$\begin{bmatrix} \dot{\boldsymbol{g}}_x(\boldsymbol{x}(t)) \\ \dot{\boldsymbol{g}}_y(\boldsymbol{x}(t)) \end{bmatrix} = \boldsymbol{K} \begin{bmatrix} \boldsymbol{g}_x(\boldsymbol{x}(t)) \\ \boldsymbol{g}_y(\boldsymbol{x}(t)) \end{bmatrix}, \tag{23}$$

where $\boldsymbol{K} \in \mathbb{R}^{(n_d+n_y)\times(n_d+n_y)}$ is the augmented Koopman operator that builds a link between the system state variables, $\boldsymbol{x}$, and the measurement variables, $\boldsymbol{y}$, in the lifted space. Now, we decompose the augmented Koopman operator $\boldsymbol{K}$ as

$$\boldsymbol{K} = \begin{bmatrix} \boldsymbol{K}_x & \boldsymbol{K}_{xy} \\ \boldsymbol{K}_{yx} & \boldsymbol{K}_y \end{bmatrix} = \begin{bmatrix} \boldsymbol{K}_{xxy} \\ \boldsymbol{K}_{yxy} \end{bmatrix}, \tag{24}$$

where $\boldsymbol{K}_x \in \mathbb{R}^{n_d \times n_d}$, $\boldsymbol{K}_{xy} \in \mathbb{R}^{n_d \times n_y}$, $\boldsymbol{K}_{yx} \in \mathbb{R}^{n_y \times n_d}$, and $\boldsymbol{K}_y \in \mathbb{R}^{n_y \times n_y}$ are the decomposed Koopman operators. Also, let us denote $\boldsymbol{K}_{xxy} = [\boldsymbol{K}_x\ \boldsymbol{K}_{xy}] \in \mathbb{R}^{n_d \times (n_d+n_y)}$, $\boldsymbol{K}_{yxy} = [\boldsymbol{K}_{yx}\ \boldsymbol{K}_y] \in \mathbb{R}^{n_y \times (n_d+n_y)}$, and $n_a = n_d + n_y$ for simplicity. Consequently, we have

$$\dot{\boldsymbol{g}}_x(\boldsymbol{x}) = \boldsymbol{K}_x \boldsymbol{g}_x(\boldsymbol{x}) + \boldsymbol{K}_{xy}\boldsymbol{g}_y(\boldsymbol{x}) = \boldsymbol{K}_{xxy} \cdot \boldsymbol{g}(\boldsymbol{x}), \tag{25}$$

$$\dot{\boldsymbol{g}}_y(\boldsymbol{x}) = \boldsymbol{K}_{yx} \boldsymbol{g}_x(\boldsymbol{x}) + \boldsymbol{K}_y\boldsymbol{g}_y(\boldsymbol{x}) = \boldsymbol{K}_{yxy} \cdot \boldsymbol{g}(\boldsymbol{x}). \tag{26}$$

This reveals the link between different Koopman observable sets that can be mapped through the decomposed Koopman operator.

Proposition: The augmented Koopman operator associated with its decomposed Koopman operator can map any initial conditions to the system measurements at any moment.

Proof: Since the augmented Koopman operator still holds for

$$\begin{aligned} \boldsymbol{g}(\boldsymbol{x}_k) = \boldsymbol{K} \cdot \boldsymbol{g}(\boldsymbol{x}_{k-1}) &= \boldsymbol{K}^2 \cdot \boldsymbol{g}(\boldsymbol{x}_{k-2}) \\ &= \cdots = \boldsymbol{K}^k \cdot \boldsymbol{g}(\boldsymbol{x}_0), \end{aligned} \tag{27}$$

we can substitute (27) into (26) to get

$$\boldsymbol{g}_y(\boldsymbol{x}_{k+1}) = \boldsymbol{K}_{yxy} \cdot \boldsymbol{K}^k \cdot \boldsymbol{g}(\boldsymbol{x}_0). \tag{28}$$

Also, since we have $\boldsymbol{g}_y(\boldsymbol{x}_{k+1}) = \boldsymbol{h}(\boldsymbol{x}_{k+1})$, we get

$$\begin{aligned} \boldsymbol{y}_{k+1} =& \boldsymbol{h}(\boldsymbol{x}_{k+1}) = \boldsymbol{K}_{yxy} \cdot \boldsymbol{K}^{k} \cdot \boldsymbol{g}(\boldsymbol{x}_0), \\ \boldsymbol{y}_{k} =& \boldsymbol{h}(\boldsymbol{x}_{k}) = \boldsymbol{K}_{yxy} \cdot \boldsymbol{K}^{k-1} \cdot \boldsymbol{g}(\boldsymbol{x}_0), \\ & \vdots \\ \boldsymbol{y}_{2} =& \boldsymbol{h}(\boldsymbol{x}_{2}) = \boldsymbol{K}_{yxy} \cdot \boldsymbol{K} \cdot \boldsymbol{g}(\boldsymbol{x}_0), \\ \boldsymbol{y}_{1} =& \boldsymbol{h}(\boldsymbol{x}_{1}) = \boldsymbol{K}_{yxy} \cdot \boldsymbol{g}(\boldsymbol{x}_0). \end{aligned} \tag{29}$$

This completes the proof.

B. Koopman-based Observability Analysis

Now, let us present the detailed procedure to derive the observability matrix in the Koopman canonical coordinates.

First, since in the Koopman space, $\boldsymbol{x} = \boldsymbol{g}(\boldsymbol{x})$ as given by (20), its corresponding state-measurement relationship is given by (5), that is,

$$\mathcal{Y}(t) = \left[\boldsymbol{y}(t), \dot{\boldsymbol{y}}(t), \cdots, \boldsymbol{y}^{(n_a-1)}(t)\right]^T. \tag{30}$$

This leads to its associated observability matrix as

$$\boldsymbol{O}(t) = \frac{\partial \mathcal{Y}(t)}{\partial \boldsymbol{x}(t)} = \begin{bmatrix} \frac{\partial \boldsymbol{y}(t)}{\partial \boldsymbol{x}} \\ \frac{\partial \dot{\boldsymbol{y}}(t)}{\partial \boldsymbol{x}} \\ \vdots \\ \frac{\partial \boldsymbol{y}^{(n_a-1)}(t)}{\partial \boldsymbol{x}} \end{bmatrix}. \tag{31}$$

Similarly, since $\boldsymbol{x} = \boldsymbol{g}(\boldsymbol{x})$, (31) can also be expressed as

$$\boldsymbol{O}(t) = \frac{\partial \mathcal{Y}(t)}{\partial \boldsymbol{g}(\boldsymbol{x}(t))} = \begin{bmatrix} \frac{\partial \boldsymbol{y}(t)}{\partial \boldsymbol{g}} \\ \frac{\partial \dot{\boldsymbol{y}}(t)}{\partial \boldsymbol{g}} \\ \vdots \\ \frac{\partial \boldsymbol{y}^{(n_a-1)}(t)}{\partial \boldsymbol{g}} \end{bmatrix}, \tag{32}$$

where $\boldsymbol{y}^n(t) = \boldsymbol{h} \cdot (\underbrace{\boldsymbol{f} \cdots (\boldsymbol{f}}_{n}((x))))$. Obviously, the above observability matrix is difficult to solve due to the nonlinearity of the system. Luckily, the measurement model is already preserved in our Koopman space as we specifically add the measurements as the observables $\boldsymbol{g}_y$ as given by (22). Then, using (26) and (28), we reformulate (30) as

$$\begin{aligned} \mathcal{Y}(t) &= \begin{bmatrix} \boldsymbol{g}_y \\ \dot{\boldsymbol{g}}_y \\ \vdots \\ \boldsymbol{g}_y{}^{(n_d+n_y-1)} \end{bmatrix} = \begin{bmatrix} \boldsymbol{K}_{yxy} \cdot \boldsymbol{K}^{k-1} \cdot \boldsymbol{g}(\boldsymbol{x}(0)) \\ \boldsymbol{K}_{yxy} \cdot \boldsymbol{K}^{k} \cdot \boldsymbol{g}(\boldsymbol{x}(0)) \\ \vdots \\ \boldsymbol{K}_{yxy} \cdot \boldsymbol{K}^{k+n_a-2} \cdot \boldsymbol{g}(\boldsymbol{x}(0)) \end{bmatrix} \\ &= \begin{bmatrix} \boldsymbol{K}_{yxy} \cdot \boldsymbol{K}^{-1} \cdot \boldsymbol{g}(\boldsymbol{x}(t)) \\ \boldsymbol{K}_{yxy} \cdot \boldsymbol{K}^{0} \cdot \boldsymbol{g}(\boldsymbol{x}(t)) \\ \vdots \\ \boldsymbol{K}_{yxy} \cdot \boldsymbol{K}^{n_a-2} \cdot \boldsymbol{g}(\boldsymbol{x}(t)) \end{bmatrix}. \end{aligned} \tag{33}$$

Therefore, its associated observability matrix given by (31) can be written as

$$\boldsymbol{O}(t) = \frac{\partial \mathcal{Y}(t)}{\partial \boldsymbol{g}(\boldsymbol{x}(t))} = \begin{bmatrix} \boldsymbol{K}_{yxy} \cdot \boldsymbol{K}^{-1} \\ \boldsymbol{K}_{yxy} \\ \vdots \\ \boldsymbol{K}_{yxy} \cdot \boldsymbol{K}^{n_a-2} \end{bmatrix}. \tag{34}$$

Till now, we have derived the Koopman-based observability matrix, $\boldsymbol{O}(t)$, which allows us to check the observability by evaluating its rank. Here, it is worth pointing out that since the decomposed Koopman operator and augmented Koopman operator are constant, so does the associated Koopman observability matrix. This also greatly alleviates the complexity of the observability analysis for a nonlinear dynamical system.

C. Degree of Koopman Observability

Although the rank of the abovementioned Koopman observability matrix, $\boldsymbol{O}(t)$, determines whether the system is observable or not, it provides a "yes or no" answer that does not indicate the degree of observability of the system. It turns out that several indexes can be used, such as the determinant, spectral radius, trace, and condition number, to name a few [13], [42], [43]. Interestingly, these indexes can be naturally extended to the Koopman-based observability analysis framework.

Following the tradition of power system dynamic observability analysis [14]–[17], we select in this paper the condition number as an index of system observability since it is a measure of the "invertibility" of a matrix [44]. It is defined as

$$c(\boldsymbol{O}) = \frac{\sigma_{\max}(\boldsymbol{O})}{\sigma_{\min}(\boldsymbol{O})}, \tag{35}$$

where $\sigma_{\min}(\boldsymbol{O})$ and $\sigma_{\max}(\boldsymbol{O})$ are the smallest and the largest singular value, respectively. It is obtained through the factorization of the observability matrix as

$$\boldsymbol{O} = \boldsymbol{U}_o \boldsymbol{\Sigma}_o \boldsymbol{V}_o{}^T, \tag{36}$$

where $\boldsymbol{U}_o^T \boldsymbol{U}_o = \boldsymbol{I}$, $\boldsymbol{V}_o^T \boldsymbol{V}_o = \boldsymbol{I}$, and the columns of $\boldsymbol{U}_0(\boldsymbol{V}_o)$ are the orthonormal eigenvectors. The entries of the diagonal matrix $\boldsymbol{\Sigma}_o$ are the square roots of the eigenvalues with respect to $\boldsymbol{U}_o(\boldsymbol{V}_o)$ in the descending order. Its associated singular value is the square root denoted by $\sigma_i(\boldsymbol{O})$ of the Koopman observability matrix, $\boldsymbol{O}$. Since this index is defined as the ratio of the largest singular value to the smallest one, the larger the condition number, $c(\boldsymbol{O})$, is, the weaker the observability of the system becomes. Note that the degree of observability can be assessed using this criterion for the unobservable system.

Furthermore, the contribution level of a measurement to the degree of observability of a dynamical system is defined as the change in the system observability degree due to the measurement inclusion in the system. Interestingly, in the next section, simulation results in power systems showed that measurements have different contribution levels.

D. Implementation of the Proposed Method

Using the above Koopman-based method, the detailed procedure for analyzing the observability of a power system dynamic model is described in Algorithm 1. Here, we would like to point out that the selection of the observables for the power system dynamic model remains an open problem. Note that there are different ways to get $\boldsymbol{g}_x(\boldsymbol{x})$ while the selection of $\boldsymbol{g}_y(\boldsymbol{x})$ remains unchanged since it is simply obtained from the measurement model in a deterministic way as shown by (21). Also, we suggest removing negligible Koopman observables from $\boldsymbol{g}_x(\boldsymbol{x})$ while $\boldsymbol{g}_y(\boldsymbol{x})$ are fully retained. This is because

these observables contribute little to the Koopman operator, $\boldsymbol{K}$. It turns out that they can be easily detected using the built-in `rref` function in MATLAB® platform. Once they are removed, we re-estimate $\boldsymbol{K}$ and $\boldsymbol{K}_{yxy}$ for the sake of consistency.

Finally, we emphasize that our proposed Koopman observability matrix is able to provide, as a return, valuable guidance for the selection of the observables in the Koopman operator. It is necessary to select the Koopman observables that ensure better observability for the state estimation-related research, e.g., the Koopman Kalman filter [45], to name a few.

Algorithm 1 Koopman-based Observability Analysis of a Power System Dynamic Model

Implement the power system dynamic model (3) as well as its measurement model (4);
Collect the dynamic system response data from the selected power system dynamic model;
Select the Koopman observables for $\boldsymbol{g}_x(\boldsymbol{x}) \in \mathbb{R}^{n_d}$ as taking the measurement functions (4) as observables $\boldsymbol{g}_y(\boldsymbol{x}) \in \mathbb{R}^{n_y}$ directly;
Apply EDMD method to estimate the augmented Koopman operator, $\boldsymbol{K} \in \mathbb{R}^{n_a \times n_a}$;
Decompose the augmented Koopman operator, $\boldsymbol{K}$, to obtain its decomposed one, namely $\boldsymbol{K}_{yxy} \in \mathbb{R}^{n_y \times (n_a)}$;
Formulate the Koopman observability matrix, $\boldsymbol{O}$, using $\boldsymbol{K}$ and $\boldsymbol{K}_{yxy}$ as shown in (34);
check the rank of the observability matrix;
Calculate the degree of observability;
while unobservable **do**
    Determine negligible Koopman observables in the Koopman observability matrix.
    Remove the negligible Koopman observables and re-estimate $\boldsymbol{K}$ and $\boldsymbol{K}_{yxy}$;
    Calculate the degree of observability;
end while
Analyze the power system dynamic observability analysis results.

E. Further Discussions

Now, we would like to mention that the reason we select the EDMD method instead of the aforementioned DMD method or the modified Arnoldi method [32], [33], [39], [46], is because the key step to formulate the proposed augmented Koopman operator relies on (22). Therefore, the DMD method is not appropriate for the formulation adopted in this article. Besides, the EDMD method improves upon the classical DMD method by the inclusion of a flexible choice of dictionary of observables that spans a finite-dimensional subspace on which the Koopman operator can be better approximated [40]. This not only improves the accuracy of the Koopman method but also expands the applicability of the Koopman formalism.

Another interesting point that merits further discussion is that, although we evaluate the degree of observability by the condition number of the Koopman observability matrix, there is also an alternative strategy proposed in a recently published paper [47]. The latter paper aims to identify a relatively small subset of state variables that reflects the most dominant Koopman mode. In this manner, the observability of a given Koopman mode is analyzed under a selected set of observables elaborated in the perturbed Koopman mode analysis as suggested by Hernández-Ortega and Messina [48]. This method is meaningful since, in practice, system operators tend to be more interested in monitoring the most dominant modes. However, our application and focus are different in that we are more on the dynamic observability analysis that can assist in the DSE, for which the associated estimation accuracy and the numerical stability may not only be accounted for by the dominant mode. But, the relationship between this alternative strategy with our proposed method deserves further exploration and will be investigated in future work.

V. Simulation Results

In this section, we demonstrate the performance of the proposed method when applied to various test systems, including a small nonlinear system and several IEEE test systems with different synchronous generator models [49].

A. Application to a Simple Nonlinear System

1) The Koopman Method: Let us apply the proposed method to a simple two-dimensional nonlinear system, which is governed by

$$\begin{cases} \dot{x}_1 = \alpha(x_1 - x_2^2), \\ \dot{x}_2 = \beta x_2, \end{cases} \tag{37}$$

where the initial conditions are given by $x_1(0) = -1$ and $x_2(0) = 2$ and the parameters are given by $\alpha = -1$ and $\beta = -0.05$. Here, the simulation time is set to 3 seconds and the time step is set to 0.01 s. Let us select different measurement models to test the observability and the associated degree of observability of this nonlinear system as illustrated in Table I. Let us also consider five different Koopman observable sets. For each set, we use four different Koopman observables, $\boldsymbol{g}_x(\boldsymbol{x})$, which are *Hermite polynomials* in the linear form, the decoupled quadratic, the quadratic form[2] and a complicated form includes the quadratic form with an extra set of a cosine function and a sine function for each state variable separately. For example, for the Observable Set 4, the measurement model is chosen to be $y_1 = x_1$, $y_2 = x_2$, and $y_3 = {x_1}^2$. This means that $\boldsymbol{g}_y(\boldsymbol{x})$ includes a set of observables given by $\{x_1, x_2, x_1^2\}$.

From the case studies of Observable Set 1 and 2, we can see that the x_1 demonstrates stronger observability as a measure when compared to that of x_2 since its associated Koopman condition number, $c(\boldsymbol{O})$, always takes a smaller value, namely stronger observability. This is confirmed by the plots of the trajectories of x_1 and x_2 that are displayed in Fig.1. From these plots, we observe that the evolution of the measurement of x_1 exhibits a larger variation than that of the measurement of x_2. This also means that the former measurement has a higher sensitivity, which typically leads to higher observability. This

[2]Here, the decoupled quadratic form neglects the coupled second-order terms, yielding $\{1, x_1, x_2, {x_1}^2 - 1, {x_2}^2 - 1\}$ as $\boldsymbol{g}_x(\boldsymbol{x})$. As for the coupled quadratic form, it is given by $\{1, x_1, x_2, x_1x_2, {x_1}^2 - 1, {x_2}^2 - 1\}$.

TABLE I
ASSESSMENT OF THE PROPOSED METHOD FOR DIFFERENT MEASUREMENT CONFIGURATIONS AND DIFFERENT KOOPMAN OBSERVABLE SETS

Observable Set 1 using $\{x_1\}$ as measurement				
Koopman	Linear	Qua-decop	Quadratic	Complicated
Observable	Yes	Yes	Yes	No
$c(\boldsymbol{O})$	$3.90e+03$	$2.13e+11$	$1.77e+11$	$3.2e+15$
Observable Set 2 using $\{x_2\}$ as measurement				
Koopman	Linear	Qua-decop	Quadratic	Complicated
Observable	No	No	No	No
$c(\boldsymbol{O})$	$1.46e+17$	$2.72e+16$	$2.78e+18$	$1.99e+17$
Observable Set 3 using $\{x_1, x_2\}$ as measurement				
Koopman	Linear	Qua-decop	Quadratic	Complicated
Observable	Yes	Yes	Yes	Yes
$c(\boldsymbol{O})$	$8.60e+01$	$1.33e+09$	$3.88e+08$	$6.38e+11$
Observable Set 4 using $\{x_1, x_2, {x_1}^2\}$ as measurement				
Koopman	Linear	Qua-decop	Quadratic	Complicated
Observable	Yes	Yes	Yes	Yes
$c(\boldsymbol{O})$	$5.60e+01$	$1.19e+03$	$1.55e+02$	$4.64e+08$
Observable Set 5 using $\{x_1, x_2, {x_2}^2\}$ as measurement				
Koopman	Linear	Qua-decop	Quadratic	Complicated
Observable	Yes	Yes	Yes	Yes
$c(\boldsymbol{O})$	$2.60e+03$	$2.59e+07$	$1.51e+07$	$2.84e+10$

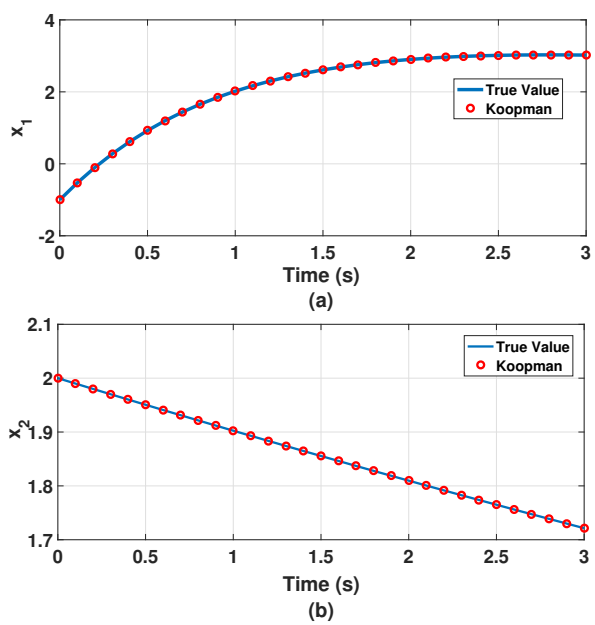

Fig. 1. Plots of the predicted system states using the proposed augmented Koopman operator compared with the actual trajectories.

further verifies the rationale of our proposed method to some extent.

From the case studies of Observable Set 1 and 3, we verify that the increase in the number of measurements will increase the degree of observability. By further comparing the case studies of Observable Set 4 and 5, we found that by incorporating low-observability-related measurement, e.g., ${x_2}^2$ in Observable Set 5, the degree of observability tends to be smaller than that with a high-observability-related measurement, e.g., ${x_1}^2$ in Observable Set 4.

Finally, let us point out that the selection of different Koopman observables leads to different degrees of observability. Typically, the observable vector, $\boldsymbol{g}_x(\boldsymbol{x})$, with more elements tends to lead to a system with a relatively smaller degree of observability. This makes sense since more observable functions are lifting the original system to a higher-dimensional Koopman space while the measurement model remains unchanged. However, there is no guarantee that the system measurements are still sensitive to the variations of all the Koopman observables and, therefore, which may result in weaker observability. This brings an interesting remark: although the more Koopman observables, the better the system's nonlinear dynamics will be, it will bring some challenges to the system observability in the Koopman space. Indeed, if we suppose that we have an infinite number of Koopman observables in an infinite-dimensional Koopman space, it is not possible for a state estimator to estimate all of them while the measurement set remains finite and unchanged.

2) The Lie-derivative Method: Here, let us analyze some simulation results of the traditional Lie-derivative method [14], [15], [29]. Specifically, we test 5 different measurements as listed in Table. I, namely $\{x_1\}$, $\{x_2\}$, $\{x_1, x_2\}$, $\{x_1, x_2, x_1^2\}$, and $\{x_1, x_2, x_2^2\}$, respectively. The simulation results are taken as a benchmark to validate our proposed Koopman method. It is found that both methods provide the same results. They both identify that the measurement of $\{x_2\}$ leads to an unobservable case while the other four cases are observable. Besides, as a key difference, the Koopman approach does not need to know any model parameters, such as α and β in (37). This can be an obvious advantage of the data-driven Koopman method compared with the model-based lie-derivative method when parameter uncertainties exist.

TABLE II
OBSERVABILITY ANALYSIS COMPARED WITH THE LIE-DERIVATIVE METHOD

Observable	Set 1	Set 2	Set 3	Set 4	Set 5
Lie-derivative	Yes	No	Yes	Yes	Yes
Koopman	Yes	No	Yes	Yes	Yes

3) Test under noise: In practice, the measured data inevitably contains noise. Although the aforementioned Koopman approach does not address the noise issue, the Koopman operator can still be approximated using the EDMD method under noisy conditions. This is articulated by Williams *et al.* [40], who state that if the data provided to the EDMD method are generated by a Markov process instead of by a deterministic system, the algorithm approximates the eigenfunctions of the Kolmogorov backward equation. The latter can be considered as a *stochastic Koopman operator* while the detailed procedure of the EDMD method remains unchanged. Therefore, it is important to discuss the performance of the proposed method under measurement noise. Let us assume that the latter is an independent identically distributed Gaussian process with a standard deviation of 0.01 and 0.001, respectively, for different test groups. The associated simulation results based on different measurements and noise are shown in Table III.

From the simulation results, we observe that since the generated noise is random, the values of the degree of observability, $c(\boldsymbol{O})$, vary a little bit under the same settings. However, the general trend used to assess the degree of observability does not change. For example, similar to the noise-free test conditions, the Observable set 2 has a smaller degree of observability compared with the Observable set 1 under different noise and measurement settings. Also, when we increase the measurement number as shown in the Observable set 3 and the Observable set 6, the degree of observability increases accordingly. Besides, when a noise is added, the general degree of the Koopman observability increases as compared with the noise-free conditions. This makes sense since the numerical stability of the EDMD approximated Koopman operator increases when a small noise is included. This will, therefore, alleviate the ill-conditioning problem of the Koopman observability matrix and, in turn, improve the degree of observability, to some extent. Consequently, the above simulations show that the proposed method can also be applied to noisy conditions while providing valuable information for the dynamic observability analysis.

TABLE III
ASSESSMENT OF THE PROPOSED METHOD UNDER DIFFERENT MEASUREMENT NOISE

Observable Set 1 using $\{x_1\}$ as measurement with 1% noise			
Koopman	Linear	Qua-decop	Quadratic
$c(\boldsymbol{O})$	$7.93e+01$	$1.97e+05$	$2.67e+04$
Observable Set 2 using $\{x_2\}$ as measurement with 1% noise			
Koopman	Linear	Qua-decop	Quadratic
$c(\boldsymbol{O})$	$2.3150e+05$	$1.0250e+06$	$9.9015e+06$
Observable Set 3 using $\{x_1, x_2\}$ as measurement with 1% noise			
Koopman	Linear	Qua-decop	Quadratic
$c(\boldsymbol{O})$	5.95	$3.76e+02$	$1.36e+03$
Observable Set 4 using $\{x_1\}$ as measurement with 0.1% noise			
Koopman	Linear	Qua-decop	Quadratic
$c(\boldsymbol{O})$	$3.39e+03$	$3.44e+06$	$2.98e+05$
Observable Set 5 using $\{x_2\}$ as measurement with 0.1% noise			
Koopman	Linear	Qua-decop	Quadratic
$c(\boldsymbol{O})$	$1.13e+06$	$2.32e+08$	$2.946e+06$
Observable Set 6 using $\{x_1, x_2\}$ as measurement with 0.1% noise			
Koopman	Linear	Qua-decop	Quadratic
$c(\boldsymbol{O})$	6.42	$5.95e+03$	$2.92e+03$

B. Application to the IEEE 9-Bus System

1) The Koopman Method: Let us further evaluate the performance of the proposed method when it is applied to the IEEE 9-bus system using the classical generator model. The topology and parameters of this model are provided in [44, ch. 5]. The transmission line between Bus 8 and Bus 9 is opened to induce a disturbance in the system. The simulation duration is set to be 20 s. Similar to previous test cases, we use three different sets of Koopman observables, which are *Hermite polynomials* in the decoupled quadratic, the quadratic form, and a complicated form that includes extra kernel functions for each state variable, namely δ, and ω, separately. Here, as shown in Table. IV, we analyze the Koopman observability for different types of PMUs measuring V, θ, P_e and Q_e, at 60 frames per second. Also, to make the comparison fair, we assume that we have only one set of PMUs placed on each generator terminal bus, a placement that ensures an equal number of each measurement type.

TABLE IV
ASSESSMENT OF THE PROPOSED METHOD USING DIFFERENT MEASUREMENT SELECTIONS AND DIFFERENT KOOPMAN OBSERVABLES IN THE IEEE 9-BUS SYSTEM

Observable Set 1 using V as measurement			
Koopman	Qua-decop	Quadratic	Complicated
Observable	Yes	Yes	No
$c(\boldsymbol{O})$	$1.11e+09$	$1.00e+09$	$2.79e+13$
Observable Set 2 using θ as measurement			
Koopman	Qua-decop	Quadratic	Complicated
Observable	Yes	Yes	Yes
$c(\boldsymbol{O})$	$7.18e+06$	$1.52e+08$	$5.73e+11$
Observable Set 3 using P as measurement			
Koopman	Qua-decop	Quadratic	Complicated
Observable	Yes	Yes	Yes
$c(\boldsymbol{O})$	$2.27e+07$	$3.66e+08$	$1.63e+12$
Observable Set 4 using Q as measurement			
Koopman	Qua-decop	Quadratic	Complicated
Observable	Yes	Yes	Yes
$c(\boldsymbol{O})$	$4.75e+07$	$2.86e+07$	$3.62e+11$
Observable Set 5 using $\{P, Q\}$ as measurement			
Koopman	Qua-decop	Quadratic	Complicated
Observable	Yes	Yes	Yes
$c(\boldsymbol{O})$	$2.17e+06$	$9.71e+06$	$1.80e+09$
Observable Set 6 using $\{P, Q, V\}$ as measurement			
Koopman	Qua-decop	Quadratic	Complicated
Observable	Yes	Yes	Yes
$c(\boldsymbol{O})$	$2.0242e+09$	$2.8352e+09$	$1.0299e+16$

From the case studies of Observable Set 1 to 4, we conclude that different collections of observables lead to different values of the degree of system observability. Furthermore, measuring at every generator bus the voltage magnitude, V, leads to the lowest observability compared with measuring the voltage phase angle, θ, or the real power, P_e, or the reactive power, Q_e. Interestingly, this is consistent with the conclusion made in [45], which does not recommend the selection of the generator voltage magnitudes as observables.

From the case studies of Observable Set 3, 4, and 5, we infer that the increase in the number of measurements will generally increase the degree of observability. However, this is not always true, as the case studies of Observable Set 5 and 6 show. Indeed, in these studies, the simulations reveal that if a measurement with a very low degree of observability is added in addition, the overall degree of observability will decrease to some extent. Therefore, we do not necessarily have a greater degree of observability if we place more measurements in the system. In fact, the overall degree of observability quantified by the conditional number will only increase when the measurements with relatively strong observability are added.

Finally, note that in general, the more Koopman observables one selects, the lower the degree of observability tends to be.

In other words, with more Koopman observables, we estimate more states of the system in canonical Koopman coordinates accordingly while the number of measurements remains unchanged, which decreases the measurement redundancy.

2) Computing efficiency of the Koopman-based method compared to that of the lie-derivative method: Now, let us further compare the computing time of the Koopman-based method to that of the Lie-derivative method. Here, it is worth pointing out that, although known to be accurate under nonlinear conditions, the Lie-derivative method is also known to have serious computing speed issues that prohibit its application to large-scale dynamic systems [14], [17]. In our test case, we find that the computational efficiency of our Koopman method significantly surpasses the Lie-derivative method, as shown in Table V. This further demonstrates the advantage of the proposed Koopman method.

TABLE V
COMPARISON OF THE COMPUTING EFFICIENCY

Method	The Lie-derivative Method	The Koopman Method
Computing Time	25 min 19 sec	0.129 sec

C. Application to the 39-bus New England System

1) Tests without noise: Let us further test the proposed method by applying it to a larger system, namely, the New England 39-bus system, while using the classical generator model. Here, a set of PMUs are placed at the generator terminals so that they provide metered values of V, θ, P, and Q. To analyze the dynamics of the power systems subjected to a disturbance, we open the transmission line between Bus 15 and Bus 16. Let us first test the degree of observability measured by the condition number, $c(\boldsymbol{O})$, for different numbers of measurements and for different Koopman observables. The latter are *Hermite polynomials* in the decoupled quadratic form, the quadratic form, and a complicated form that includes extra kernel functions. The other settings remain unchanged in the previous case.

The simulation results are shown in Table VI. For PMU Set 1, we place the PMUs on all the PV buses. For PMU Set 2, we increase the number of PMUs by placing them on all buses for comparison. Here we come to the following conclusions.

First, from the first two rows of each PMU set, we can see that PMU Set 2 exhibits a stronger degree of observability than PMU Set 1. This reveals that with more measuring devices, we achieve better observability when using the same Koopman observables. Also, with more Koopman observables, it is more likely to obtain an unobservable system in the Koopman space.

Second, since the dimension of the system increases, the dimension of the lifted Koopman space will increase accordingly. However, it is not easy to select the Koopman observables that guarantee the observability of the system with insufficient measurement as shown in PMU Set 1. This is clearly reflected in the third row of TableVI, where the left number is the rank of the Koopman observability matrix while the right one is its full rank number. In contrast, although with more Koopman observables, PMU Set 2 demonstrates better observability due to the incorporation of more measurement devices in the system.

Finally, although the incorporation of a large number of Koopman observables, in general, better characterizes the nonlinearity of the system, it may jeopardize its observability to some extent. Fortunately, it is not difficult to adjust the selected Koopman observables in order to achieve system observability. As we discussed in Section IV-D, we can remove negligible Koopman observables having little contribution to the Koopman operator in order to make the observability matrix full rank. Once done, we can re-estimate its adjusted condition number, denoted as $c_a(\boldsymbol{O})$, as shown in the fourth row of TableVI. Note that a higher degree of observability is achieved now.

TABLE VI
ASSESSMENT OF THE PROPOSED METHOD USING DIFFERENT NUMBERS OF PMUS AND DIFFERENT KOOPMAN OBSERVABLES IN THE IEEE 39-BUS TEST SYSTEM

PMU Set 1: Meters placed only on PV Buses			
Koopman	Qua-decop	Quadratic	Complicated
Observable	No	No	No
$c(\boldsymbol{O})$	$1.44e+15$	$4.43e+14$	$3.00e+15$
$Rank$	$51/77$	$213/230$	$224/266$
$c_a(\boldsymbol{O})$	$2.38e+08$	$2.73e+11$	$8.35e+11$
PMU Set 2: Meters Placed on All Buses			
Koopman	Qua-decop	Quadratic	Complicated
Observable	Yes	Yes	No
$c(\boldsymbol{O})$	$1.22e+11$	$6.16e+10$	$4.75e+11$
$Rank$	$135/135$	$288/288$	$319/324$
$c_a(\boldsymbol{O})$	–	–	$2.03e+11$

2) Tests with noise: Let us further test the performance of the proposed method in the New England test system considering the noise. Here, we select different measurements and different observables to check the degree of observability. Again, we assume that the noise is an independent and identically distributed Gaussian process with a standard deviation of 0.001. The simulation results are shown in Table VII.

Compared with the tests that ignore the noise that is shown in Table VI, the simulation results show that the degree of observability, in general, increases since a small noise can alleviate the ill-conditioning problem of the Koopman observability matrix as we discussed in Section V-A3. Also, as we increase the number of the measurements from Test 1 to 4, it is found that the degree of the observability increases accordingly and this holds for different types of observables. This further verifies the rationale of the proposed method in the dynamic observability analysis. Also, we find that, in general, the more observables are selected, the weaker the dynamic observability tends to be in the Koopman space. This matches the conclusion in the noise-free test conditions as discussed in Section V-C1. However, more observables typically bring a better characterization of nonlinear dynamics. Therefore, it is indeed a valuable topic to further investigate the trade-off between the degree of observability and the number of Koopman observables in the lifted Koopman space.

3) Tests with different fault locations: Now, let us further test our proposed observability assessment method under different fault locations. Here, we test 4 different fault locations

TABLE VII
ASSESSMENT OF THE PROPOSED METHOD IN THE IEEE 39-BUS TEST SYSTEM CONSIDERING THE NOISE

Test 1: P only on PV Buses			
Koopman	Qua-decop	Quadratic	Complicated
$c(\boldsymbol{O})$	$3.1895e+04$	$5.8410e+11$	$7.0796e+12$
$Rank$	$47/47$	$200/200$	$223/236$
$c_a(\boldsymbol{O})$	–	–	$3.7752e+11$
Test 2: P and Q only on PV Buses			
Koopman	Qua-decop	Quadratic	Complicated
$c(\boldsymbol{O})$	$2.3069e+03$	$1.4884e+07$	$3.9769e+07$
$Rank$	$57/57$	$210/210$	$246/246$
$c_a(\boldsymbol{O})$	–	–	–
Test 3: Meters placed only on PV Buses			
Koopman	Qua-decop	Quadratic	Complicated
$c(\boldsymbol{O})$	594.7470	$4.7178e+04$	$9.4612e+04$
$Rank$	$77/77$	$230/230$	$266/266$
$c_a(\boldsymbol{O})$	–	–	–
Test 4: Meters placed on All Buses			
Koopman	Qua-decop	Quadratic	Complicated
$c(\boldsymbol{O})$	300.9542	$2.5950e+03$	$4.0423e+03$
$Rank$	$135/135$	$288/288$	$324/324$
$c_a(\boldsymbol{O})$	–	–	–

under different observables as shown in Fig. 2. Accordingly, the different transmission lines are tripped for each test. We assume that the PMUs are placed on all the buses while the other settings remain unchanged with previous case studies. The detailed simulation results are shown in Table VIII.

From the simulations, we observe that different fault locations lead to different degrees of observability given different Koopman observables. This makes sense since different fault locations stimulate various dynamic responses of the power system, which intrinsically reveal different values of the observability matrix. Again, we find that more observables typically bring weaker observability in the Koopman space under different fault locations. This also matches the conclusions in the previous case studies. One interesting property that we find is that, although different observables are selected, tripping the transmission line 17-27 yields the highest observability while tripping the transmission line 15-16 leads to the lowest one among all the 4 test locations. Therefore, we can say that different power system topologies reveal different degrees of observability for the dynamic responses.

D. Application to the 39-bus New England system with traditional generators and converter interfaced generations

It is worth pointing out that our proposed method is quite general and is not limited to a specific synchronous generator model. Indeed, modern power systems are evolving with more and more renewable energy generations [50]–[52]. This motivates us to further demonstrate our proposed method in the New England test system with both traditional generators and converter-interfaced generations (CIGs). As shown in Fig.3, we added two CIGs on Bus 5 and 21 separately. The other settings for the traditional synchronous generators remain unchanged with the ones indicated in Section V-C.

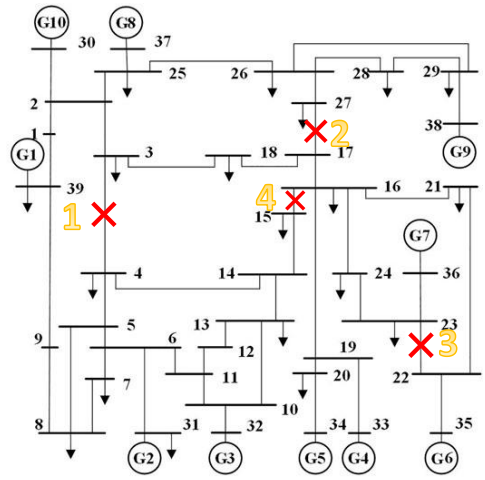

Fig. 2. Plots of Different Events in the IEEE 39-Bus System.

TABLE VIII
ASSESSMENT OF THE PROPOSED METHOD IN THE IEEE 39-BUS TEST SYSTEM CONSIDERING DIFFERENT FAULT LOCATIONS

Test 1: Trip Transmission Line 3-4			
Koopman	Qua-decop	Quadratic	Complicated
$c(\boldsymbol{O})$	302.7931	$1.9672e+03$	$2.5974e+03$
$Rank$	$135/135$	$288/288$	$324/324$
$c_a(\boldsymbol{O})$	–	–	–
Test 2: Trip Transmission Line 17-27			
Koopman	Qua-decop	Quadratic	Complicated
$c(\boldsymbol{O})$	198.1149	$1.2841e+03$	$1.5136e+03$
$Rank$	$135/135$	$288/288$	$324/324$
$c_a(\boldsymbol{O})$	–	–	–
Test 3: Trip Transmission Line 22-23			
Koopman	Qua-decop	Quadratic	Complicated
$c(\boldsymbol{O})$	226.8987	$1.5611e+03$	$1.6745e+03$
$Rank$	$135/135$	$288/288$	$324/324$
$c_a(\boldsymbol{O})$	–	–	–
Test 4: Trip Transmission Line 15-16			
Koopman	Qua-decop	Quadratic	Complicated
$c(\boldsymbol{O})$	307.9542	$2.5950e+03$	$4.0423e+03$
$Rank$	$135/135$	$288/288$	$324/324$
$c_a(\boldsymbol{O})$	–	–	–

We follow the CIG model adopted in [50], [53], which includes a virtual inertia control design. More specifically, its inertia control is displayed in Fig.4. (a) while the associated Phase-Locked Loop (PLL) is depicted in Fig.4. (b).

The detailed dynamic model is described next[3]. For the CIG

[3]Here, we would like to mention that the proposed method is currently relying on the continuous functions to approximate the Koopman operator as one reviewer has pointed out. Therefore, if the CIG model is using much more detailed models, such as the switching model for the power electronics devices, then the discrete features in the dynamics are hard to be captured. Besides, since the switching frequency in power electronics is very high, it is also difficult for the PMU to capture its fast dynamics. Therefore, we do not recommend using the approximate method to apply the switching model directly. Another important issue that deserves to be discussed is that the current definition of dynamic observability (5) is based on the derivation of continuous functions. Therefore, if the discrete variables from power electronics devices are considered, the derivative-based analysis tools, including the Lie-derivative method, cannot be applied directly as well. This is indeed an important and difficult problem that deserves further investigation.

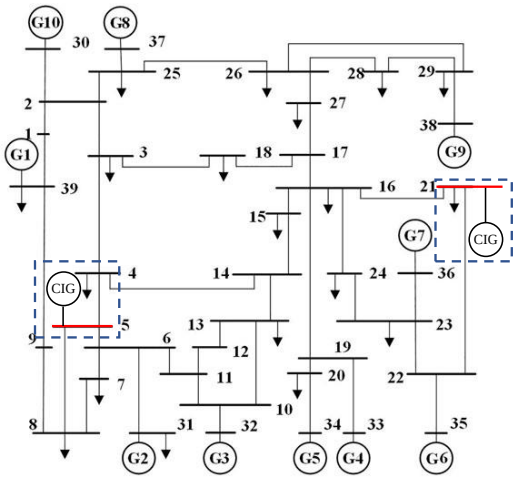

Fig. 3. Plot of the IEEE 39-Bus System with the added converter-interfaced-generators (CIG).

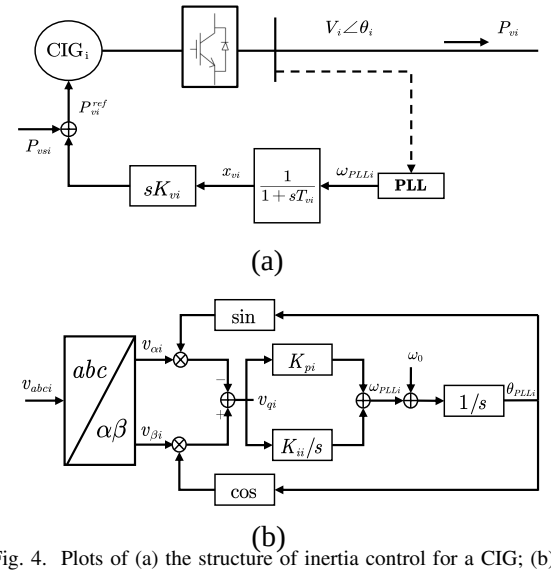

Fig. 4. Plots of (a) the structure of inertia control for a CIG; (b) the internal structure of a PLL.

shown in Fig.4. (a), we have

$$\dot{x}_{vi} = \frac{1}{T_{Vi}}(\omega_{PLL_i} - x_{vi}), \tag{38}$$

$$\dot{P}_{vi} = \frac{1}{T_{Pi}}(P_{vsi} - K_{vi}\dot{x}_{vi} - P_{vi}), \tag{39}$$

where the $\dot{x}_{vi}$ is the intermediate state variable from the metered frequency and $\dot{P}_{vsi}$, $\dot{P}_{vi}^{ref}$ and $\dot{P}_{vi}$ are the reference value under no virtual inertia control, active power reference, and active power of the ith CIGs. As for $\dot{P}_{vi}$, it can also be obtained through

$$\dot{P}_{vi} = P_{vi}^{ref} + K_{vi}\dot{x}_{vi}. \tag{40}$$

T_{Vi}, T_{Pi}, and K_{vi} are the control parameters. Here, K_{vi} is used to emulate the virtual inertia H_{vi} via $K_{vi} = 2H_{vi}$. ω_{PLL_i} is the deviation of the measured frequency from the nominal frequency, ω_0.

For the PLL displayed in Fig.4. (b), its dynamic model is governed by

$$\dot{\theta}_{PLL_i} = \omega_{PLL_i} + \omega_0, \tag{41}$$

$$\dot{x}_{PLL_i} = v_{qi} = V_i sin(\theta_i - \theta_{PLL_i}), \tag{42}$$

$$\omega_{PLL_i} = K_{pi}v_{qi} + K_{ii}x_{PLL_i}. \tag{43}$$

Here, θ_i and θ_{PLL_i} denote the bus voltage angle and PLL voltage angle respectively. x_{PLL_i} represents the intermediate variable and v_{qi} is the q-axis voltage. K_{pi} and K_{ii} are the control parameters. All the aforementioned parameter values of these two GIGs with inertia control are provided in Appendix A.

Now, we select different measurements and different observables to test the degree of observability. Also, we assume the noise to be identical, independent Gaussian noise with a standard deviation of 0.001. For Test 1, PMUs are placed only on PV buses. For Test 2, we increase the meters number by placing them on all the buses. The simulation results are given in Table IX.

From the simulations, we observe that even if the CIG is considered, we can still apply our Koopman method to assess the dynamic observability of the power system. Also, the proposed Koopman method can identify a higher degree of observability for Test 2 compared with that of Test 1 under the same settings. This makes sense since we have more PMUs in Test 2, which enhances the observability. Besides, we would like to emphasize that the proposed method does have good computational efficiency, which allows the simulations to be completed in a short period of time. Also, in the test system considering the CIGs, the previous conclusion that the more observables are selected, the weaker the dynamic observability tends to be in the Koopman space still holds here.

TABLE IX
ASSESSMENT OF THE PROPOSED METHOD USING CLASSICAL GENERATOR MODELS AND CIGS WITH VIRTUAL INERTIA CONTROL IN THE IEEE 39-BUS TEST SYSTEM

Test 1: Meters placed only on PV buses			
Koopman	Qua-decop	Quadratic	Complicated
Rank	$101/101$	$332/332$	$376/376$
$c(\boldsymbol{O})$	$2.141e+03$	$2.29e+05$	$2.719e+05$
Time	$1.47s$	$7.14s$	$13.8s$
Test 2: Meters placed on all buses			
Koopman	Qua-decop	Quadratic	Complicated
Rank	$155/155$	$386/386$	$430/430$
$c(\boldsymbol{O})$	$8.63e+02$	$1.077e+04$	$1.095e+04$
Time	$1.75s$	$23.355s$	$29.88s$

E. Test System with a Detailed Generator Model

Here, let us further test our proposed method in the New-England system with a detailed generator model, namely the 9th-order synchronous generator with the IEEE-DC1A exciter and the TGOV1 turbine-governor. For this case, we assume that we have PMUs placed only at PV buses to estimate the system states. Since we have 9 state variables for each generator while the measurement number remains unchanged with our tests given in Group 1 of Table. VI, it is foreseeable

that it tends to be a more challenging task. Also, we are using the *Hermite polynomials* in the decoupled quadratic form for this test case since it contains much fewer observables compared with that of the coupled quadratic form for this high-dimension dynamic system. To make a better comparison, we further adopt different measurements. The simulation results are given in Table X leads to the following conclusions.

TABLE X
ASSESSMENT OF THE PROPOSED METHOD USING DETAILED GENERATOR MODELS IN THE IEEE 39-BUS TEST SYSTEM

PMU Set 1: Meters placed only on PV Buses			
Measure	$\{P, Q\}$	$\{P, Q, V, \theta\}$	$\{P, Q, \omega\}$
Observable	No	No	No
$c(\boldsymbol{O})$	$1.35e+17$	$6.64e+16$	$2.94e+17$
$Rank$	$76/201$	$149/279$	$94/211$
$c_a(\boldsymbol{O})$	$4.44e+08$	$4.24e+08$	$1.13e+08$

First, comparing the conditional number, $c(\boldsymbol{O})$, in Table. X of $\{P, Q, V, \theta\}$ with that of Table. VI, we found that although the measurement placements are exactly the same, the degree of observability drops significantly for the ones using a detailed generator model. This makes sense since it is more difficult to infer more state variables using the same PMU sets. This verifies the rationale of our proposed method.

Second, by only placing PMUs on the PV buses, we found that for our test cases with the detailed generator model, it is difficult to obtain a full rank observability matrix by casually selecting the Koopman observables. Therefore, it is quite necessary for us to adjust the Koopman observables when the dimension of the system states increases. Here, by comparing the $c(\boldsymbol{O})$ and $c_a(\boldsymbol{O})$, we found that the degree of observability increases significantly under different measurement settings. Also, this further demonstrates the trade-off between the number of the Koopman observables and the degree of observability. Here, it is interesting to find that the PMU set with $\{P, Q, \omega\}$ demonstrates the best observability for its $c_a(\boldsymbol{O})$. This is consistent with the suggestions made by Netto in [45] for the Koopman observable selection of a Kalman filter.

Finally, let us mention that the proposed Koopman observability method is based on the linear Koopman operator that yields quite good computational efficiency. For instance, for the New England system, we can complete the simulations in a few seconds. This is indeed an attractive computing speed when carrying out dynamic observability analysis.

F. Further Discussions

1) Discussions on Outlier Issues: As mentioned in [54], in practice, three different types of outliers exist, namely, structural outliers, innovation outliers, and observation (measurement) outliers. Since the proposed Koopman approach is a data-driven method that does not rely on the accuracy of the model, it can avoid the influences from the structural outliers intrinsically. However, the proposed method is not robust to measurement outliers because it makes use of the DMD method [39] or the EDMD method, which is based on least-squares estimators that exhibit an unbounded influence function [54]–[56]. So, it comes as no surprise that research work has been devoted to developing robust tools, such as the generalized-maximum-likelihood estimator-based DMD method [57]. Here, since the approximation of our proposed augmented Koopman operator relies on the EDMD method, it is worth further exploration on developing a robust EDMD method to robustify the Koopman approximation procedure.

2) Discussions on the robustness of the singular value decomposition (SVD)): Another issue related to the robustness of the proposed method comes from the SVD procedure. It is also well-known that the conventional SVD is indeed a least-squares method that is vulnerable to outliers, such as sparks, missing data, etc. [58]. Therefore, this might also lead to biased estimation results of the degree of observability when outliers are presented. Facing this issue, although we do not develop a robust SVD method in this paper, it deserves further attention to improve the robustness of the proposed method by adopting a robust version of the SVD as suggested in [58]–[60].

3) Observable selection: The observable selection problem remains an open problem in power systems that attracts lots of attention from researchers [61], [62]. Here, when the problem comes to the dynamic observability problem as we addressed in this article, we find that this is an even more interesting problem since the observables' numbers and locations also have an impact on the degree of the observability. Therefore, it is possible for us to enhance the overall observability of the power system dynamics by properly selecting the Koopman observables. If a systematic procedure is developed, it will not only balance the accuracy and computing efficiency in the Koopman observability analysis but it will help to guide the optimal meter placement for the dynamic state estimation of the power system [13]. We will take it as valuable future work.

VI. CONCLUSIONS AND FUTURE WORK

In this paper, we propose a Koopman-based observability analysis framework for analyzing the observability of a power system nonlinear dynamical model. We formulate an augmented Koopman operator that reveals the link between the system states and the measurements in a data-driven manner. The performances of the proposed method are verified in multiple test systems. As a future work, we will develop systematic methods for selecting the Koopman observables in a more systematic way. Also, we will explore the development of robust EDMD and SVD methods to improve the performance of the proposed method in presence of outliers.

ACKNOWLEDGMENT

The authors would like to thank Dr. Marcos Netto for interesting discussions on the Koopman operator as applied to power systems. Furthermore, careful reading and helpful suggestions from the editor and anonymous reviewers markedly improved the manuscript.

Appendix A
Parameters of the Converter-Interfaced-Generators

The detailed model parameters of the two CIGs with virtual inertia control are provided in Table. XI as shown below. The control parameters are set as the same as [53].

TABLE XI
PARAMETERS OF CIGS WITH VIRTUAL INERTIA CONTROL

Parameters	CIG_1	CIG_2
T_{vi}	1	1
T_{pi}	0.2	0.2
K_P	10	10
K_i	500	500
H_v	20	25

.

References

[1] Y.-Y. Liu, J.-J. Slotine, and A.-L. Barabási, "Observability of complex systems," *Proceedings of the National Academy of Sciences*, vol. 110, no. 7, pp. 2460–2465, 2013.

[2] T. Baldwin, L. Mili, M. Boisen, and R. Adapa, "Power system observability with minimal phasor measurement placement," *IEEE Transactions on Power Systems*, vol. 8, no. 2, pp. 707–715, 1993.

[3] R. Nuqui and A. Phadke, "Phasor measurement unit placement techniques for complete and incomplete observability," *IEEE Transactions on Power Delivery*, vol. 20, no. 4, pp. 2381–2388, 2005.

[4] B. Gou and R. G. Kavasseri, "Unified pmu placement for observability and bad data detection in state estimation," *IEEE Transactions on Power Systems*, vol. 29, no. 6, pp. 2573–2580, 2014.

[5] B. Gou and A. Abur, "A direct numerical method for observability analysis," *IEEE Transactions on Power Systems*, vol. 15, no. 2, pp. 625–630, 2000.

[6] Y. Liao, "Fault location observability analysis and optimal meter placement based on voltage measurements," *Electr. Power Syst. Res*, vol. 79, no. 7, pp. 1062–1068, 2009.

[7] M. Korkali and A. Abur, "Optimal deployment of wide-area synchronized measurements for fault-location observability," *IEEE Transactions on Power Systems*, vol. 28, no. 1, pp. 482–489, 2013.

[8] S. Bhela, V. Kekatos, and S. Veeramachaneni, "Enhancing observability in distribution grids using smart meter data," *IEEE Trans. Smart Grid*, vol. 9, no. 6, pp. 5953–5961, Nov. 2018.

[9] S. Bhela, V. Kekatos, and S. Veeramachaneni, "Smart inverter grid probing for learning loads: Part I—Identifiability analysis," *IEEE Trans. Power Syst.*, vol. 34, no. 5, pp. 3527–3536, Sep. 2019.

[10] G. Tian *et al.*, "Neural-network-based power system state estimation with extended observability," *Journal of Modern Power Systems and Clean Energy*, vol. 9, no. 5, pp. 1043–1053, 2021.

[11] Y. Peng, Z. Wu, W. Gu, S. Zhou, and P. Liu, "Optimal micro-pmu placement for improving state estimation accuracy via mixed-integer semidefinite programming," *Journal of Modern Power Systems and Clean Energy*, pp. 1–11, 2022.

[12] G. Cavraro, A. Bernstein, V. Kekatos, and Y. Zhang, "Real-time identifiability of power distribution network topologies with limited monitoring," *IEEE Control Syst. Lett.*, vol. 4, no. 2, pp. 325–330, Apr. 2020.

[13] J. Qi, K. Sun, and W. Kang, "Optimal PMU placement for power system dynamic state estimation by using empirical observability Gramian," *IEEE Trans. Power Syst.*, vol. 30, no. 4, pp. 2041–2054, Jul. 2015.

[14] A. Rouhani and A. Abur, "Observability analysis for dynamic state estimation of synchronous machines," *IEEE Trans. Power Syst.*, vol. 32, no. 4, pp. 3168–3175, Jul. 2017.

[15] G. Wang, C. Liu, N. Bhatt, E. Farantatos, and M. Patel, "Observability of nonlinear power system dynamics using synchrophasor data," *Int. Trans. Electr. Energy Syst.*, vol. 26, no. 5, pp. 952–967, May 2016.

[16] Z. Zheng *et al.*, "Derivative-free observability analysis of a stochastic dynamical system," *IEEE Trans. Network Sci. Eng.*, vol. 8, no. 3, pp. 2426–2437, Jul.–Sep. 2021.

[17] Z. Zheng *et al.*, "Observability analysis of a power system stochastic dynamical model using a derivative-free approach," *IEEE Trans. Power Syst.*, 2021.

[18] J. Zhao *et al.*, "Power system dynamic state estimation: Motivations, definitions, methodologies, and future work," *IEEE Transactions on Power Systems*, vol. 34, no. 4, pp. 3188–3198, 2019.

[19] Z. Huang, P. Du, D. Kosterev, and S. Yang, "Generator dynamic model validation and parameter calibration using phasor measurements at the point of connection," *IEEE Transactions on Power Systems*, vol. 28, no. 2, pp. 1939–1949, 2013.

[20] Y. Xu, L. Mili, X. Chen, M. Korkali, and L. Min, "A Bayesian approach to real-time dynamic parameter estimation using phasor measurement unit measurement," *IEEE Trans. Power Syst.*, vol. 35, no. 2, pp. 1109–1119, Mar. 2020.

[21] S. Wang, R. Huang, Z. Huang, and R. Fan, "A robust dynamic state estimation approach against model errors caused by load changes," *IEEE Transactions on Power Systems*, vol. 35, no. 6, pp. 4518–4527, 2020.

[22] A. Rouhani and A. Abur, "Constrained iterated unscented kalman filter for dynamic state and parameter estimation," *IEEE Transactions on Power Systems*, vol. 33, no. 3, pp. 2404–2414, 2018.

[23] Y. Xu *et al.*, "Response-surface-based Bayesian inference for power system dynamic parameter estimation," *IEEE Trans. Smart Grid*, vol. 10, no. 6, pp. 5899–5909, Nov. 2019.

[24] C. T. Chen, *Linear System Theory and Design*. New York: Holt, Rinehart and Winston, 1984.

[25] M. Netto, J. Zhao, and L. Mili, "A robust extended kalman filter for power system dynamic state estimation using pmu measurements," in *2016 IEEE Power and Energy Society General Meeting (PESGM)*. IEEE, 2016, pp. 1–5.

[26] J. Zhao, M. Netto, and L. Mili, "A robust iterated extended kalman filter for power system dynamic state estimation," *IEEE Transactions on Power Systems*, vol. 32, no. 4, pp. 3205–3216, 2016.

[27] P. W. Sauer, M. A. Pai, and J. H. Chow, *Power system dynamics and stability: with synchrophasor measurement and power system toolbox*. John Wiley & Sons, 2017.

[28] J. Gauthier and G. Bornard, "Observability for any u (t) of a class of nonlinear systems," *IEEE Transactions on Automatic Control*, vol. 26, no. 4, pp. 922–926, 1981.

[29] R. Hermann and A. Krener, "Nonlinear controllability and observability," *IEEE Transactions on automatic control*, vol. 22, no. 5, pp. 728–740, 1977.

[30] T. L. Baldwin, L. Mili, M. B. Boisen, and R. Adapa, "Power system observability with minimal phasor measurement placement," *IEEE Trans. Power Syst.*, vol. 8, no. 2, pp. 707–715, May 1993.

[31] I. Mezić, "Spectral properties of dynamical systems, model reduction and decompositions," *Nonlinear Dynamics*, vol. 41, no. 1, pp. 309–325, 2005.

[32] C. W. Rowley, I. Mezić, S. Bagheri, P. Schlatter, and D. S. Henningson, "Spectral analysis of nonlinear flows," *Journal of fluid mechanics*, vol. 641, pp. 115–127, 2009.

[33] Y. Susuki and I. Mezić, "Nonlinear Koopman modes and coherency identification of coupled swing dynamics," *IEEE Trans. Power Syst.*, vol. 26, no. 4, pp. 1894–1904, 2011.

[34] Y. Susuki and I. Mezić, "Nonlinear koopman modes and power system stability assessment without models," *IEEE Transactions on Power Systems*, vol. 29, no. 2, pp. 899–907, 2013.

[35] X. Li, C. Mishra, S. Chen, Y. Wang, and J. De La Ree, "Determination of parameters of time-delayed embedding algorithm using koopman operator-based model predictive frequency control," *CSEE Journal of Power and Energy Systems*, vol. 7, no. 6, pp. 1140–1151, 2021.

[36] X. Gong, X. Wang, and G. Joos, "An online data-driven method for microgrid secondary voltage and frequency control with ensemble koopman modeling," *IEEE Transactions on Smart Grid*, 2022.

[37] M. Netto, Y. Susuki, and L. Mili, "Data-driven participation factors for nonlinear systems based on koopman mode decomposition," *IEEE control systems letters*, vol. 3, no. 1, pp. 198–203, 2018.

[38] Y. Xu, M. Netto, and L. Mili, "Propagating parameter uncertainty in power system nonlinear dynamic simulations using a koopman operator-based surrogate model," *IEEE Transactions on Power Systems*, 2022.

[39] P. J. Schmid, "Dynamic mode decomposition of numerical and experimental data," *Journal of fluid mechanics*, vol. 656, pp. 5–28, 2010.

[40] M. O. Williams, I. G. Kevrekidis, and C. W. Rowley, "A data-driven approximation of the Koopman operator: Extending dynamic mode decomposition," *J Nonlinear Sci*, vol. 25, no. 6, pp. 1307–1346, 2015.

[41] S. Klus, P. Koltai, and C. Schütte, "On the numerical approximation of the perron-frobenius and koopman operator," *Journal of Computational*

Dynamics, vol. 3, no. 1, pp. 51–79, 2016.

[42] A. K. Singh and J. Hahn, "Determining optimal sensor locations for state and parameter estimation for stable nonlinear systems," *Industrial & engineering chemistry research*, vol. 44, no. 15, pp. 5645–5659, 2005.

[43] V. Lystianingrum, B. Hredzak, V. G. Agelidis, and V. S. Djanali, "Observability degree criteria evaluation for temperature observability in a battery string towards optimal thermal sensors placement," in *2014 IEEE Ninth International Conference on Intelligent Sensors, Sensor Networks and Information Processing (ISSNIP)*. IEEE, 2014, pp. 1–6.

[44] M. L. Crow, *Computational methods for electric power systems*. Crc Press, 2002.

[45] M. Netto and L. Mili, "A robust data-driven koopman kalman filter for power systems dynamic state estimation," *IEEE Transactions on Power Systems*, 2018.

[46] A. Hasnain *et al.*, "Learning perturbation-inducible cell states from observability analysis of transcriptome dynamics," *Nature Communications*, vol. 14, no. 1, p. 3148, 2023.

[47] M. A. Hernández-Ortega, A. Chakrabortty, A. R. Messina, and C. M. Rergis, "Nonlinear koopman observability measures on subsets of power system state variables," in *2021 60th IEEE Conference on Decision and Control (CDC)*. IEEE, 2021, pp. 4222–4227.

[48] M. Hernández-Ortega and A. Messina, "Nonlinear power system analysis using koopman mode decomposition and perturbation theory," *IEEE Transactions on Power Systems*, vol. 33, no. 5, pp. 5124–5134, 2018.

[49] A. Pai, *Energy function analysis for power system stability*. Springer Science & Business Media, 1989.

[50] J. Ma *et al.*, "Research on the impact of dfig virtual inertia control on power system small-signal stability considering the phase-locked loop," *IEEE Transactions on Power Systems*, vol. 32, no. 3, pp. 2094–2105, 2016.

[51] K. Liao *et al.*, "A sliding mode based damping control of dfig for interarea power oscillations," *IEEE Transactions on Sustainable Energy*, vol. 8, no. 1, pp. 258–267, 2016.

[52] K. Liao, Y. Xu, Z. He, and Z. Y. Dong, "Second-order sliding mode based pq coordinated modulation of dfigs against interarea oscillations," *IEEE Transactions on Power Systems*, vol. 32, no. 6, pp. 4978–4980, 2017.

[53] J. Guo, X. Wang, and B.-T. Ooi, "Estimation of inertia for synchronous and non-synchronous generators based on ambient measurements," *IEEE Transactions on Power Systems*, vol. 37, no. 5, pp. 3747–3757, 2021.

[54] M. A. Gandhi and L. Mili, "Robust Kalman filter based on a generalized maximum-likelihood-type estimator," *IEEE Trans. Signal Process.*, vol. 58, no. 5, pp. 2509–2520, May 2010.

[55] L. Mili, G. Steeno, F. Dobraca, and D. French, "A robust estimation method for topology error identification," *IEEE Trans. Power Syst.*, vol. 14, no. 4, pp. 1469–1476, Nov. 1999.

[56] M. Korkalı and A. Abur, "Robust fault location using least-absolute-value estimator," *IEEE Trans. Power Syst.*, vol. 28, no. 4, pp. 4384–4392, Nov. 2013.

[57] A. H. Abolmasoumi, M. Netto, and L. Mili, "Robust dynamic mode decomposition," *IEEE Access*, vol. 10, pp. 65 473–65 484, 2022.

[58] L. Liu, D. M. Hawkins, S. Ghosh, and S. S. Young, "Robust singular value decomposition analysis of microarray data," *Proceedings of the National Academy of Sciences*, vol. 100, no. 23, pp. 13 167–13 172, 2003.

[59] B. Lei, Y. Soon, and E.-L. Tan, "Robust svd-based audio watermarking scheme with differential evolution optimization," *IEEE transactions on audio, speech, and language processing*, vol. 21, no. 11, pp. 2368–2378, 2013.

[60] W. Wang, Z. Dang, Y. Hu, P. Fua, and M. Salzmann, "Robust differentiable svd," *IEEE Transactions on Pattern Analysis and Machine Intelligence*, vol. 44, no. 9, pp. 5472–5487, 2021.

[61] M. Netto, Y. Susuki, V. Krishnan, and Y. Zhang, "On analytical construction of observable functions in extended dynamic mode decomposition for nonlinear estimation and prediction," in *2021 American Control Conference (ACC)*. IEEE, 2021, pp. 4190–4195.

[62] B. Lusch, J. N. Kutz, and S. L. Brunton, "Deep learning for universal linear embeddings of nonlinear dynamics," *Nature communications*, vol. 9, no. 1, p. 4950, 2018.

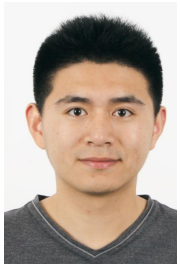

Yijun Xu (SM'21) is a professor at Southeast University, Nanjing, China. He received his Ph.D. degree from the Bradley Department of Electrical and Computer Engineering at Virginia Tech, Falls Church, VA, in December 2018. He worked as a research assistant professor at Virginia Tech-Northern Virginia Center, Falls Church, VA, in 2021. He was a postdoc associate at the same institute from 2019 to 2020. He did a computation internship at Lawrence Livermore National Laboratory, Livermore, CA, and a power engineer internship at ETAP – Operation Technology, Inc., Irvine, California, in 2018 and 2015, respectively.

His research interests include power system uncertainty quantification, uncertainty inversion, and decision-making under uncertainty. Dr. Xu is currently serving as an Associate Editor of the IET GENERATION, TRANSMISSION & DISTRIBUTION and an Associate Editor of the IET RENEWABLE POWER GENERATION. He is the co-chair of the IEEE Task Force on Power System Uncertainty Quantification and Uncertainty-Aware Decision-Making.

Qinling Wang (S'23) received the B.S. degree in Applied Physics from Shanghai University of Electric Power. She is currently working toward the M.S. degree in the School of Electrical Engineering from Southeast University, Nanjing, China, since 2022. Her research interests include modeling of power system dynamics, Koopman theory, and robust statistics.

Lamine Mili (LF'17) received the Ph.D. degree from the University of Liège, Belgium, in 1987. He is a Professor of Electrical and Computer Engineering, Virginia Tech, Blacksburg. He has five years of industrial experience with the Tunisian electric utility, STEG. At STEG, he worked in the planning department from 1976 to 1979 and then at the Test and Meter Laboratory from 1979 till 1981. He was a Visiting Professor with the Swiss Federal Institute of Technology in Lausanne, the Grenoble Institute of Technology, the École Supérieure D'électricité in France and the École Polytechnique de Tunisie in Tunisia, and did consulting work for the French Power Transmission company, RTE.

His research has focused on power system planning for enhanced resiliency and sustainability, risk management of complex systems to catastrophic failures, robust estimation and control, nonlinear dynamics, and bifurcation theory. He is the co-founder and co-editor of the *International Journal of Critical Infrastructure*. He is the chairman of the IEEE Working Group on State Estimation Algorithms and the chair of the IEEE Task Force on Power System Uncertainty Quantification and Uncertainty-Aware Decision-Making. He is a recipient of several awards including the US National Science Foundation (NSF) Research Initiation Award and the NSF Young Investigation Award.

Zongsheng Zheng (M'20) received the Ph.D. degree in electrical engineering from Southwest Jiaotong University, Chengdu, China, in 2020. During 2018-2019, he was a Visiting Scholar at the Bradley Department of Electrical and Computer Engineering at Virginia Tech-Northern Virginia Center, Falls Church, VA, USA. He is currently a Research Associate Professor at the College of Electrical Engineering, Sichuan University. His research interests include uncertainty quantification, parameter and state estimation.

Wei Gu (M'06-SM'16) received his B.S. and Ph.D. degrees in Electrical Engineering from Southeast University, China, in 2001 and 2006, respectively. From 2009 to 2010, he was a Visiting Scholar in the Department of Electrical Engineering, Arizona State University. He is now a professor at the School of Electrical Engineering, Southeast University. He is the director of the institute of distributed generations and active distribution networks.

His research interests include distributed generations and microgrids, and integrated energy systems. He is an Editor for the IEEE Transactions on Power Systems, the IET Energy Systems Integration and the Automation of Electric Power Systems (China).

Shuai Lu (S'17-M'21) received his B.S. degree in Smart Grid Information Engineering from Nanjing University of Science and Technology, Nanjing, China in 2016 and the Ph.D. degree in Electrical Engineering from Southeast University, Nanjing China, in 2021. From 2018 to 2019, he was a visiting scholar at the University of New South Wales, Sydney, Australia. He is currently a Lecture at the School of Electrical Engineering, Southeast University.

He is a Young Editorial Board Member of Applied Energy. He was selected as an Outstanding Reviewer for IEEE Transactions on Power Systems in 2020. His research interests include integrated energy systems, operations research, and data-driven techniques in power systems.

Zhi Wu (SM'22) received the M.Sc. degree in electrical engineering from the School of Electrical Engineering, Southeast University, Nanjing, China, in 2012, and the Ph.D. degree from the University of Birmingham, Birmingham, U.K., in 2016.

He is currently working as an Associate Professor with the School of Electrical Engineering at Southeast University. His research interests include renewable energy, planning, and optimization techniques.